

Parametric decay of oblique Alfvén waves in two-dimensional hybrid simulations

D. Verscharen*

*Max-Planck-Institut für Sonnensystemforschung, Max-Planck-Str. 2, 37191 Katlenburg-Lindau, Germany and
Institut für Theoretische Physik, Technische Universität Braunschweig,
Mendelssohnstr. 3, 38106 Braunschweig, Germany*

E. Marsch†

*Max-Planck-Institut für Sonnensystemforschung, Max-Planck-Str. 2, 37191 Katlenburg-Lindau, Germany and
Institut für Experimentelle und Angewandte Physik,
Christian-Albrechts-Universität Kiel, Leibnizstr. 11, 24098 Kiel, Germany*

U. Motschmann‡

*Institut für Theoretische Physik, Technische Universität Braunschweig,
Mendelssohnstr. 3, 38106 Braunschweig, Germany and
Institut für Planetenforschung, DLR, Rutherfordstr. 2, 12489 Berlin-Adlershof, Germany*

J. Müller§

*Institut für Theoretische Physik, Technische Universität Braunschweig,
Mendelssohnstr. 3, 38106 Braunschweig, Germany*

(Dated: July 19, 2012)

Certain types of plasma waves are known to become parametrically unstable under specific plasma conditions, in which the pump wave will decay into several daughter waves with different wavenumbers and frequencies. In the past, the related plasma instabilities have been treated analytically for various parameter regimes and by use of various numerical methods, yet the oblique propagation with respect to the background magnetic field has rarely been dealt with in two dimensions, mainly because of the high computational demand. Here we present a hybrid-simulation study of the parametric decay of a moderately oblique Alfvén wave having elliptical polarization. It is found that such a compressive wave can decay into waves with higher and lower wavenumbers than the pump.

I. INTRODUCTION

Monochromatic plasma waves with certain properties are known to be parametrically unstable and to decay into daughter waves in a multiple-waves interaction process [1–7]. The ubiquitous small-amplitude thermal fluctuations existing in any plasma are considered as seeds for growing daughter waves in the presence of a large-amplitude pump wave, if that has the necessary characteristics and fulfills the required instability criteria. Multiple-wave interactions provoke these instabilities. This fact directly illustrates that they are nonlinear processes by nature. The monochromatic initial condition makes the parametric decay an illustrative example compared to other nonlinear mechanisms. Therefore, it is of general interest for a better understanding of more intricate nonlinear effects in plasmas and other statistical systems ranging from classical fusion [8, 9] and space plasmas [10, 11] to more exotic media such as relativistic electron-positron plasmas [12, 13].

Following the early analytical treatments, modern numerical simulations are capable of modeling the parametric decay [14, 15] comprehensively. Kinetic simulations even allow one to investigate in detail the interactions between the participating particles and waves, and so can reveal in particular the resultant particle heating, e.g., under conditions typical for the solar corona holes [16]. This possibility has brought the parametric decay process into the focus of coronal-heating research. In the past decade, large-amplitude magnetohydrodynamic waves have also been observed directly in the solar chromosphere and corona [17]. They seem to be mainly Alfvénic, yet with a smaller slow-mode-wave compressive component, and appear intense enough to deliver via dissipation sufficient thermal energy to the coronal ions [18, 19]. This makes them a promising energy source also for the acceleration of the fast solar wind, even though the details of the dissipation and the spectral transfer are not well understood [20–22].

Most models made use of simplifications such as one-dimensional geometry. But recently, the more powerful available computers have paved the way for fully two-dimensional analyzes, including the possibility of oblique propagation of the mother and daughter waves [23, 24]. In this context there remain, however, many open physical questions. The compressive component of the fluctuations, for example, is long known to be important for the parametric decay. Yet in the oblique case, the effects

* now at: Space Science Center, Institute for the Study of Earth, Oceans, and Space, University of New Hampshire, Durham, NH 03824, USA; daniel.verscharen@unh.edu

† marsch@physik.uni-kiel.de

‡ u.motschmann@tu-braunschweig.de

§ joa.mueller@tu-bs.de

of compressibility are not well analyzed or understood. Also, the direction of propagation of the daughter-wave products and their ability for resonant wave-particle heating are still unclear. This work will address some of these aspects and issues with the aid of numerical hybrid simulations. The treated plasma gains further degrees of freedom by choosing higher dimensionality. Since natural systems are never limited to a one-dimensional geometry only, it is crucial to understand the consequences of this advancement towards a more realistic modeling. Further complications have been treated in simplified cases before, such as the influence of additional ionic species [25, 26], dusty components in the plasma [27–29], and high collision rates [30]. The present work is supposed to provide a basis for further studies of parametric instabilities under the refined conditions adapted to the particular situation.

II. NUMERICAL METHOD

The so called A.I.K.E.F. (adaptive ion-kinetic electron-fluid) code is a numerical hybrid code, which treats ions as particles following the characteristics of the Vlasov kinetic equation and electrons as a massless charge-neutralizing fluid. Hybrid codes have been successfully applied in the past to model plenty of plasma phenomena in the limit of low frequencies compared to any frequency related to the electron dynamics [31]. The dynamics of ions are appropriately simulated as long as quasi-neutrality is satisfied. These constraints are often fulfilled in space plasmas. Therefore, hybrid simulations have proven to be adequate models for effects such as micro-instabilities [32–34], the turbulent cascade [35–37], or micro-physics at planetary magnetospheres [38, 39] to name but a few examples.

The A.I.K.E.F. code has been described by Müller et al. [40] and already been used for a treatment of waves and turbulence in space plasmas [36]. The equations of motion solved for a proton are

$$\frac{d\vec{v}_p}{dt} = \frac{q_p}{m_p} \left(\vec{E} + \frac{1}{c} \vec{v}_p \times \vec{B} \right), \quad (1)$$

$$\frac{d\vec{x}_p}{dt} = \vec{v}_p, \quad (2)$$

with the velocity \vec{v}_p and the spatial location vector \vec{x}_p . We consider the Lorentz force which acts on any particle with charge q_p and mass m_p , and is due to the electric field \vec{E} and the magnetic field \vec{B} . The speed of light is denoted by c .

Concerning the electromagnetic fields involved, we use the momentum equation of the massless electron fluid to deliver the electric field as

$$\vec{E} = -\frac{1}{c} \vec{u}_e \times \vec{B} - \frac{1}{n_e e} \nabla p_e, \quad (3)$$

where the electron bulk velocity is denoted by \vec{u}_e , the number density by n_e , and its elementary charge by e .

The magnetic field is obtained from the induction equation, which means from Faraday's law,

$$\partial \vec{B} / \partial t = -c \nabla \times \vec{E}. \quad (4)$$

The electrons are assumed to be isothermal, and thus their pressure p_e depends on the electron number density according to $p_e \propto n_e$. The proton density and the proton bulk velocity \vec{u}_p are obtained as the first two moments of the proton distribution function, and quasi-neutrality connects the density of protons and electrons.

The boundaries of the simulation box are set to be periodic, and the particles are initialized with a Maxwellian velocity distribution that is shifted to the given values for the initial bulk velocities and has a width determined by the proton beta, which is set to $\beta_p = \beta_e = 0.1$. All spatial length scales are normalized and given in units of the proton inertial length, $\ell_p = c/\omega_p$, with the proton plasma frequency $\omega_p = \sqrt{4\pi n_p q_p^2 / m_p}$. All time scales are in units of the inverse proton gyro-frequency $\Omega_p = q_p B / (m_p c)$.

The two-dimensional integration box has a size of 1024×1024 cells. Each cell is filled with 500 super-particles, which represent the real number of the protons. For the vector quantities, all three components are evaluated, and a divergence-cleaning algorithm is applied to guarantee numerical stability. A constant background magnetic field of the form $\vec{B}_0 = B_0 \vec{e}_z$ is set up, and B_0 provides the normalization unit for all magnetic fields.

The initial condition is a monochromatic Alfvén/ion-cyclotron (A/IC) wave with a normalized amplitude of $b = 0.2$. Its polarization is determined by the Hall-MHD relations, since this is the low-temperature limit of the hybrid equations [41]. The wave propagates with an angle of $\vartheta = 10^\circ$ with respect to the background magnetic field. Such a wave is elliptically polarized and has an initially compressive component. The spatial domain has a size of roughly $250\ell_p \times 250\ell_p$, restricted by the periodic connection on the boundaries.

III. RESULTS

After 50 000 time steps, corresponding to the time $t = 500$, the initial wave has decayed already. The resulting two-dimensional spectrum is shown in Fig. 1. The initial oblique pump wave is still visible as a bright dot at $k_y \approx 0.06$ and $k_z \approx 0.38$. Apparently, the wave energy has mainly been transported along the initial propagation direction of the wave. It seems to have a higher power up to $k_z = 1$ in normalized units, which means that here a spectral break should be expected. There is an increased wave activity at higher k_y , and significant additional power is distributed there. At low values of k_z , two broader perpendicular patterns are visible in the side-bands of the pump.

Also, the density fluctuation spectrum in two dimensions can be calculated from the simulation data. It is

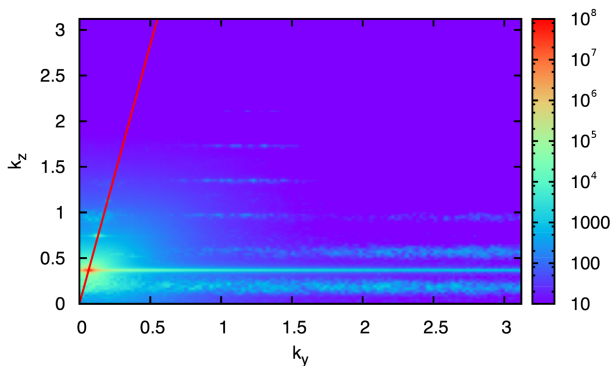


FIG. 1. (Color online) Two-dimensional power spectral density of the magnetic field fluctuations at $t = 500$. The straight line starting at the origin (red) indicates the initial propagation direction with $\vartheta = 10^\circ$. The color coding represents the power spectral density in arbitrary units.

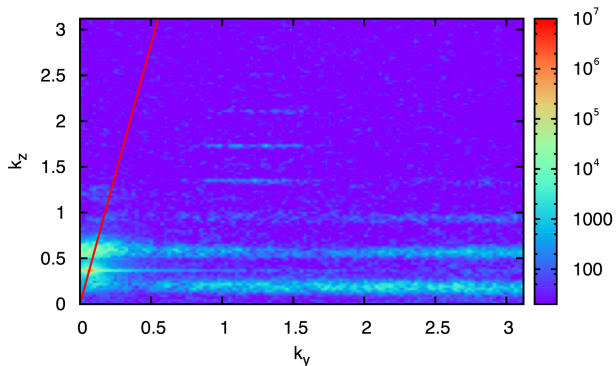


FIG. 2. (Color online) Two-dimensional power spectral density of the density fluctuations at $t = 500$. The straight line starting at the origin (red) indicates the initial propagation direction with $\vartheta = 10^\circ$. The color coding represents the power spectral density in arbitrary units.

shown in Fig. 2, which indicates that the main features visible in the magnetic fluctuation spectrum also appear in that of the density, and thus the waves possess compressive components. This is especially true for all components having a non-zero k_y . Owing to the lower overall level of these fluctuations, some filamentary intermediate structures are distinctly visible. These should be understood as representing the broad-band compressive component of the daughter waves. They occur at higher harmonics of the first side-bands, with spacing given by the parallel wavenumber of the pump wave.

To study the power distribution in more detail, the 2D Fourier transform can be cut and displayed along the direction of the initial propagation. It corresponds to a cut along the red lines in Figs. 1 and 2. The corresponding one-dimensional power spectra are shown in Figs. 3 and 4.

The initial wave is still visible in both the magnetic field fluctuations and the density fluctuations. Remem-

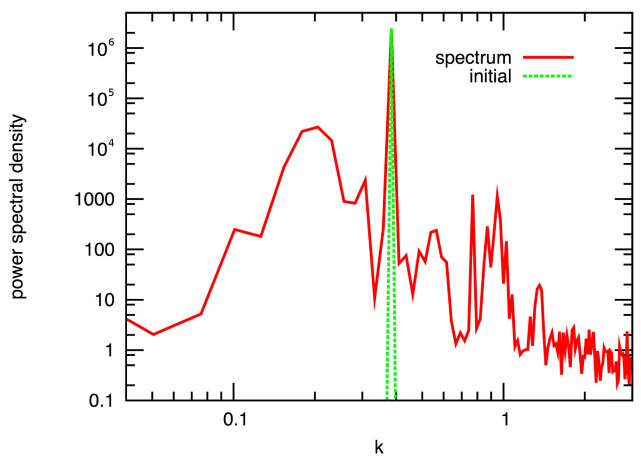


FIG. 3. (Color online) One-dimensional power spectral density for the magnetic field fluctuations at $t = 500$ along the initial direction of propagation. Additionally, the initial spectrum is shown (green dashed line).

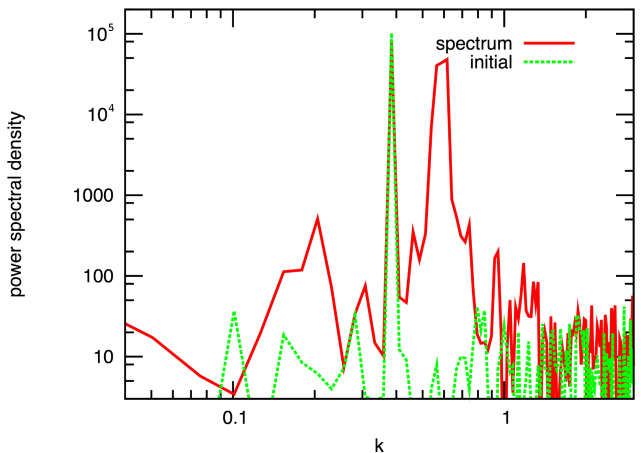


FIG. 4. (Color online) One-dimensional power spectral density for the density fluctuations at $t = 500$ along the initial direction of propagation. Additionally, the initial spectrum is shown (green dashed line).

ber that the initial wave was compressive already, due to its oblique propagation implying compressibility. The initial wave loses some energy as compared to the beginning energy. It is first spread to different wavenumbers and then dissipated at the small kinetic scales. Thus the pump wave decays to daughter waves with higher and lower wavenumbers in comparison to the initial ones.

From the simulation, the dispersion of the daughter waves can in general be determined along any direction in the (k_y, k_z) -plane. Since an enhancement of energy is seen along the initial direction of propagation (i.e., along the red line in Fig. 1), it is appropriate to calculate the dispersion along this line. Therefore, a two-dimensional spatial Fourier transform is applied, and a

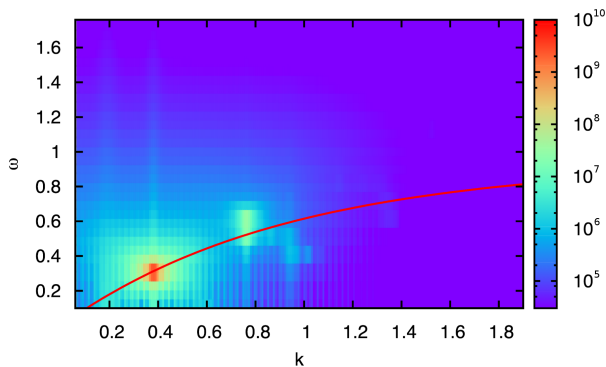


FIG. 5. (Color online) One-dimensional dispersion analysis of the magnetic field fluctuations along the direction $\vartheta = 10^\circ$ at $t = 500$. The color coding represents the power spectral density. The enhancement in power corresponds to A/IC waves propagating obliquely to the background magnetic field. The curved solid line starting at the origin (red) shows the cold-plasma dispersion relation for oblique A/IC waves with $\vartheta = 10^\circ$.

one-dimensional cut is taken along the direction $\vartheta = 10^\circ$ for 60 different time steps. They are separated by a time difference of $1/\Omega_p$ and thus allow for a temporal Fourier transformation to be performed.

The result of the spectral analysis is shown in the dispersion plot of Fig. 5. The enhanced power in the (k_y, k_z) -analysis is also very well located in the (ω, k) -plane at $k \approx 0.75$ and $\omega \approx 0.6$. Comparing this point with the theoretical cold dispersion analysis of oblique A/IC waves [42], shown as a red curve, reveals that this point is located very close to the branch of this wave mode. The width of the signal in this diagram is due to the pump wave, which has a significant amplitude compared to the background magnetic field. Therefore, waves other than the pump wave encounter an inhomogeneous guiding field due to the magnetic field of the pump wave, being superposed on the background field. The resulting total field can be understood as an effective magnetic field, around which the daughter waves propagate. This effect leads to a small broadening and shift in the dispersion analysis.

Calculations with further, moderately oblique propagation angles provide comparable results, especially the outcome that the preferred direction of the daughter wave propagation is along the initial pump wave direction.

IV. DISCUSSION AND CONCLUSIONS

The daughter waves, which are generated already after quite a short time of the nonlinear evolution, are found to be mainly aligned along the initial direction of pump wave propagation. This can be understood as a consequence of the conservation of wave momentum. In general, the wavevectors of the pump wave and the

two daughter waves have to form a vector triangle to fulfill this conservation in a three-wave process. Other arbitrary combinations would be possible for an interaction between four or even more waves [43]. However, it seems that the background magnetic field is not the most important guiding vector, but rather the initial wave propagation vector, which determines the geometry of the daughter wave vector system. The oblique-wave hybrid simulations performed by Matteini et al. [24] can also be interpreted in this sense, even though the authors favor the interpretation of a field-parallel spectral transfer. However, a major difference to their setup is our initialization with an elliptically polarized Hall-MHD pump wave, apart from the higher numerical resolution employed. The daughter waves with lower wavenumbers seem to orient themselves more perpendicular to the background field. The modulational instability can be understood as the generation mechanism here and seems to favour this direction of propagation.

An oblique wave is intrinsically compressive due to its polarization. During its evolution and decay, it is thus prone to generate a broad spectrum of compressive fluctuations. It is important to remember, though, that the amplitude of an oblique wave is in any case not arbitrary. Its intrinsic compressive effects pose an upper limit, because negative density values have to be avoided and are forbidden [44].

The dispersion relation of the decay products obtained from the oblique two-dimensional simulation shows that the related daughter waves are still A/IC waves, yet with higher wavenumber and frequency. Other wave modes such as the fast/whistler branch for example do not appear. This result is in agreement with previous treatments of the parametric decay, which have shown that the A/IC wave is a typical and major daughter product of the decay [10]. The initial oblique wave with wavenumber k_0 is prone to the decay instability with $k > k_0$ and the modulational instability with $k < k_0$. Dispersive effects let the decay instability generate A/IC waves [45]. Obviously, this effect can occur very efficiently for $k \gtrsim 0.6$. Generally, daughter waves are only excited in certain limited ranges but not on a broad range of wavenumbers. The A/IC waves, however, can easily fulfill the condition of cyclotron resonance for sufficiently high frequencies/wavenumbers. Thus, there is an upper limit for the occurrence of A/IC waves, essentially due to the onset of cyclotron damping. This leads to quite a sudden cut in the spectrum at $k \approx 0.9$. The dispersion diagram together with this typical onset of damping underlines the A/IC nature of the daughter waves.

The temperature of the particles does not increase significantly over the integration time in our simulations. This may be due to a comparably low intensity of the daughter waves, and to the limited simulation time. One-dimensional simulations have shown an increase and saturation of the particle temperatures, owing to heating by resonant wave-particle interactions [26]. The temperature in the above simulations does, however, increase if

no divergence-cleaning algorithm is applied to the magnetic fields. So, maybe a possible heating is suppressed by the present schemes, or the heating observed in previous simulations is mainly a numerical artifact. This question cannot be answered conclusively here.

ACKNOWLEDGMENTS

D. V. received financial support from the International Max Planck Research School (IMPRS) on Physical Pro-

cesses in the Solar System and Beyond. The calculations have been performed on the MEGWARE Woodcrest Cluster at the Gesellschaft für wissenschaftliche Datenverarbeitung mbH Göttingen (GWDG).

-
- [1] A. A. Galeev and V. N. Oraevskii, *Sov. Phys. Doklady* **7**, 988 (1963).
- [2] N. F. Derby, Jr., *Astrophys. J.* **224**, 1013 (1978).
- [3] M. L. Goldstein, *Astrophys. J.* **219**, 700 (1978).
- [4] C. N. Lashmore-Davies and L. Stenflo, *Plasma Phys.* **21**, 735 (1979).
- [5] H. K. Wong and M. L. Goldstein, *J. Geophys. Res.* **91**, 5617 (1986).
- [6] B. Inhester, *J. Geophys. Res.* **95**, 10525 (1990).
- [7] M. S. Ruderman and D. Simpson, *J. Plasma Phys.* **70**, 143 (2004).
- [8] G. Gnavi, R. M. O. Galvão, F. T. Gratton, and L. Gomberoff, *Phys. Rev. E* **54**, 4112 (1996).
- [9] H. A. Baldis and C. Labaune, *Plasma Phys. Contr. F.* **39**, A51 (1997).
- [10] J. A. Araneda, E. Marsch, and A. F. Viñas, *J. Geophys. Res.* **112**, 4104 (2007).
- [11] S. Tanaka, T. Ogino, and T. Umeda, *J. Geophys. Res.* **112**, A10110 (2007).
- [12] L. Gomberoff and R. M. O. Galvão, *Phys. Rev. E* **56**, 4574 (1997).
- [13] S. Matsukiyo and T. Hada, *Phys. Rev. E* **67**, 046406 (2003).
- [14] A. F. Viñas and M. L. Goldstein, *J. Plasma Phys.* **46**, 107 (1991).
- [15] J. A. Araneda, *Phys. Scripta T* **75**, 164 (1998).
- [16] J. A. Araneda, E. Marsch, and A. F.-Viñas, *Phys. Rev. Lett.* **100**, 125003 (2008).
- [17] V. M. Nakariakov and E. Verwichte, *Living Rev. Sol. Phys.* **2**, 3 (2005).
- [18] B. De Pontieu, S. W. McIntosh, M. Carlsson, V. H. Hansteen, T. D. Tarbell, C. J. Schrijver, A. M. Title, R. A. Shine, S. Tsuneta, Y. Katsukawa, K. Ichimoto, Y. Suematsu, T. Shimizu, and S. Nagata, *Science* **318**, 1574 (2007).
- [19] S. W. McIntosh, B. De Pontieu, M. Carlsson, V. Hansteen, P. Boerner, and M. Goossens, *Nature* **475**, 477 (2011).
- [20] E. Marsch, *Living Rev. Sol. Phys.* **3**, 1 (2006).
- [21] S. R. Cranmer, *Living Rev. Sol. Phys.* **6**, 3 (2009), arXiv:astro-ph/0909.2847.
- [22] L. Ofman, *Living Rev. Sol. Phys.* **7**, 4 (2010).
- [23] A. F. Viñas and M. L. Goldstein, *J. Plasma Phys.* **46**, 129 (1991).
- [24] L. Matteini, S. Landi, L. Del Zanna, M. Velli, and P. Hellinger, *Geophys. Res. Lett.* **37**, L20101 (2010).
- [25] M. K. Mishra, R. S. Chhabra, and S. R. Sharma, *Phys. Rev. E* **48**, 4642 (1993).
- [26] J. A. Araneda, Y. Maneva, and E. Marsch, *Phys. Rev. Lett.* **102**, 175001 (2009).
- [27] M. R. Amin, T. Ferdous, and M. Salimullah, *Phys. Rev. E* **53**, 2740 (1996).
- [28] M. P. Hertzberg, N. F. Cramer, and S. V. Vladimirov, *Phys. Rev. E* **69**, 056402 (2004), arXiv:physics/0601193.
- [29] P. K. Shukla, B. Eliasson, I. Kourakis, and L. Stenflo, *J. Plasma Phys.* **72**, 397 (2006).
- [30] S. V. Vladimirov and V. S. Krivitsky, *Phys. Rev. E* **47**, 1471 (1993).
- [31] D. Winske and N. Omid, *J. Geophys. Res.* **101**, 17287 (1996).
- [32] W. Daughton, S. P. Gary, and D. Winske, *J. Geophys. Res.* **104**, 4657 (1999).
- [33] S. P. Gary, L. Yin, D. Winske, L. Ofman, B. E. Goldstein, and M. Neugebauer, *J. Geophys. Res.* **108**, 1068 (2003).
- [34] M. M. Cowee, D. Winske, and S. P. Gary, *J. Geophys. Res.* **115**, A06214 (2010).
- [35] S. A. Markovskii, B. J. Vasquez, and J. V. Hollweg, *Astrophys. J.* **695**, 1413 (2009).
- [36] D. Verscharen, E. Marsch, U. Motschmann, and J. Müller, *Phys. Plasmas* **19**, 022305 (2012), arXiv:1201.2784 [physics.space-ph].
- [37] B. J. Vasquez and S. A. Markovskii, *Astrophys. J.* **747**, 19 (2012).
- [38] E. Kallio, J.-Y. Chaufray, R. Modolo, D. Snowden, and R. Winglee, *Space Sci. Rev.* **162**, 267 (2011).
- [39] J. Müller, S. Simon, Y.-C. Wang, U. Motschmann, D. Heyner, J. Schüle, W.-H. Ip, G. Kleindienst, and G. J. Pringle, *Icarus* **218**, 666 (2012).
- [40] J. Müller, S. Simon, U. Motschmann, J. Schüle, K.-H. Glassmeier, and G. J. Pringle, *Comput. Phys. Commun.* **182**, 946 (2011).
- [41] C. Vocks, U. Motschmann, and K. Glassmeier, *Ann. Geophys.* **17**, 712 (1999).
- [42] T. H. Stix, *Waves in plasmas, New York : American Institute of Physics, c1992.* (American Institute of Physics, New York, USA, 1992).
- [43] R. C. Davidson, *Methods in nonlinear plasma theory, New York, NY (USA): Academic Press (Academic Press, New York, USA, 1972).*
- [44] P. H. Yoon, *Geophys. Res. Lett.* **38**, L12105 (2011).
- [45] J. V. Hollweg, *J. Geophys. Res.* **99**, 23431 (1994).